Contrib Mineral Petrol (2000) 139: 285–297

Maxim O. Vityk · Robert J. Bodnar
Jean-Claude Doukhan

Synthetic fluid inclusions. XV. TEM investigation of plastic flow associated with reequilibration of fluid inclusions in natural quartz

Received: 5 May 1998 / Accepted: 10 February 2000

Abstract The nature and abundance of dislocations in quartz surrounding fluid inclusions were studied to obtain a better understanding of processes associated with fluid inclusion reequilibration. Synthetic fluid inclusions containing 10 wt% NaCl aqueous solution were formed in three samples at 700 °C and 5 kbar. One of the samples was quenched along an isochore to serve as a reference sample. The other two samples were quenched along a *P-T* path that generated internal pressures in excess of the confining pressure. The two samples were held at the final reequilibration *P-T* conditions of 625 °C and 2 kbar for 30 and 180 days, respectively. Following the experiments, microstructures associated with fluid inclusions were examined with the TEM. Quartz in healed fractures in the reference sample that was quenched isochorically shows a moderate dislocation activity. Quartz adjacent to reequilibrated fluid inclusions in the other two samples, however, showed a marked increase in dislocation activity compared to the un-reequilibrated sample. Deformation of the inclusion walls occurred anisotropically by expansion of mobile dislocations in their slip systems. Dislocation expansion was controlled by glide in the rhombohedral planes {1 0 1 1} that was restricted to narrow zones (≤3 μm) in the immediate vicinity of the fluid inclusion walls outside of the healed fracture plane. These plastic zones were observed after both short term (30 days) and long term (180 days) experiments and are attributed to hydrolytic weakening of quartz around fluid inclusions owing to diffusion of water into the quartz matrix during the experiment. The close spatial association of submicroscopic water bubbles with dislocations, and the rarity of water bubbles in the reference sample, show clearly that in both the 30 and 180 day experiments reequilibration involves water loss from the fluid inclusions. Our results indicate that synthetic fluid inclusions in this study recover (chemically and volumetrically), even at relatively fast experimental loading rates, such that internal stresses never reach the point of brittle failure. The driving force for fluid inclusion deformation involves two related mechanisms: plastic deformation of hydrolytically weakened wet quartz in the healed fracture, and water leakage associated with preexisting and strain-induced dislocations.

M. O. Vityk[1] · R. J. Bodnar (✉)
Fluids Research Laboratory, Department of Geological Sciences, Virginia Tech, Blacksburg, VA 24061 USA
E-mail: bubbles@vt.edu

J.-C. Doukhan
Laboratoire Structure and Propriétés Etat Solide, Université Sciences and Technologies de Lille, F-59655 Villeneuve d'Ascq-Cedex, France

Present Address:
[1]ExxonMobil Upstream Research Company, P.O. Box 2189, Houston, TX 77252-2189, USA

Editorial responsibility: J. Touret

Introduction

Larson et al. (1973) suggested that anomalously high homogenization temperatures of fluid inclusions in fluorite reported earlier were the result of inclusion volume increases generated during sample preparation and/or heating tests. These workers coined the term "*stretching*" to describe this behavior. Soon, many other papers were published which described inclusion reequilibration caused by laboratory heating at 1 atmosphere confining pressure (e.g., Leroy 1979; Swanenberg 1980; Pêcher 1981; Bodnar and Bethke 1984; Gratier and Jenatton 1984; Guilhaumou et al. 1987; Prezbindowski and Larese 1987; Bodnar et al. 1989; Wanamaker and Evans 1989) or during freezing (Lawler and Crawford 1983). Other studies described inclusion reequilibration at elevated confining pressure (e.g., Poland 1982; Pêcher and Boullier 1984; Boullier et al. 1989; Sterner and Bodnar 1989; Vityk and Bodnar 1995a, b). In the studies listed above, it was generally assumed that stretching involved only a change in the inclusion volume, with no loss of fluid from the inclusion. Other workers have investigated

compositional changes and/or mass loss during fluid inclusion reequilibration, both in the laboratory and in nature (e.g., Hall and Bodnar 1990; Bakker and Jansen 1990, 1991, 1993, 1994; Hall and Sterner 1993, 1995; Cordier et al. 1994; Kotel'nikova 1994; Mavrogenes and Bodnar 1994; Barker 1995; Johnson and Hollister 1995; Sterner et al. 1995; Vityk et al. 1995). These workers used the term "*leakage*" to describe this behavior.

In nature (and in the laboratory), fluid inclusion reequilibration at high T and low loading rates might include plasticity accommodated by glide and climb, with both being assisted by water diffusion in wet quartz. These processes involve both volume change *and* fluid loss, suggesting that inclusion stretching and leakage are related. Consider, for example, high P-T reequilibration of fluid inclusions under conditions of tectonic decompression. Under these conditions, the inclusions might undergo a volume increase (stretching or decrepitation) related to internal overpressure. However, diffusion of water into the surrounding quartz is probably required to initiate and facilitate the process, as dry natural quartz is virtually undeformable (Griggs and Blacic 1964, 1965). That is, dry quartz can only respond to an applied stress by fracturing – it cannot deform plastically. However, once water diffuses into the surrounding quartz, the quartz becomes ductile as a result of hydrolytic weakening, and can undergo plastic deformation much more easily (e.g., Kerrich 1976; Wilkins and Barkas 1978; Boullier et al. 1989; Kronenberg et al. 1986; Gerretsen et al. 1993; Cordier et al. 1994). The nucleation and propagation of mobile dislocations associated with plastic deformation extracts some water from fluid inclusions (pipe diffusion along the dislocation cores) and carries this water away from inclusions under the action of differential stress (e.g., Hollister 1990; Bakker and Jansen 1990, 1991; Cordier et al. 1994). Thus, stretching of inclusion walls by dislocation multiplication must involve some loss of water from the inclusion. Diffusion of water into the surrounding quartz, in turn, enhances inclusion plasticity which promotes fluid density changes associated with stretching.

Stretching and decrepitation (or leakage) have in the past been considered to involve two different deformational mechanisms which result in different changes to the original fluid inclusion. Figure 1 is an attempt to relate the various observations, environments and mechanisms associated with these two reequilibration processes. Thus, stretching (type of reequilibration) is associated with plastic deformation (mechanism) in a low strain environment. There is generally no detectable loss of fluid during stretching (observation), except for small amounts of hydrogen which may be lost by diffusion (mechanism; cf., Mavrogenes and Bodnar 1994). Decrepitation, on the other hand, involves the complete loss of water by advection along fractures resulting from brittle deformation in a high strain environment. Figure 1 suggests that there is a continuum between stretching and decrepitation, which represent the two

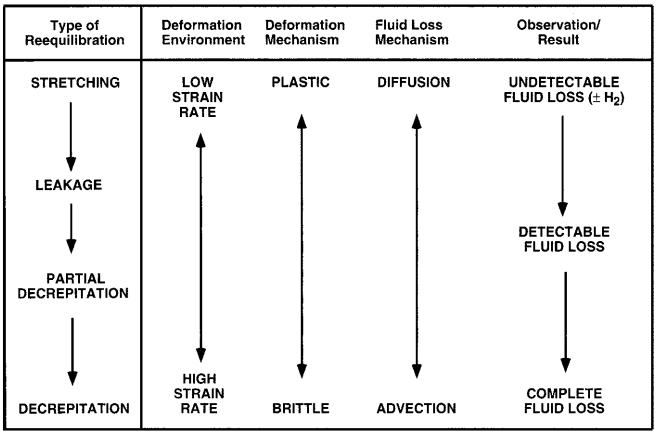

Fig. 1 Schematic representation of the relationship between different types of fluid inclusion reequilibration (stretching, leakage, decrepitation) and the environment of deformation (strain rate), the mechanisms of deformation (plastic vs brittle) and fluid loss (diffusion vs advection), and the amount of fluid lost from the inclusion during deformation (undetectable to complete). According to these relationships, stretching is associated with plastic deformation in a low strain environment, where undetectable amounts of fluid may be lost from the inclusion by diffusion. Conversely, decrepitation is associated with brittle deformation in a high strain environment, with partial to complete loss of fluid by advection along fractures

end-members of reequilibration behavior. Thus, an inclusion which stretches by plastic deformation in a low strain environment with no loss of fluid may begin to lose fluid (leak) along dislocations and/or microfractures if the strain rate increases. This type of reequilibration is often referred to as *partial decrepitation*, and the fluid loss is often detectable through microthermometric analysis (cf., Hall and Sterner 1993; Audédat and Günther 1999). The same inclusion may eventually decrepitate with loss of all fluid by explosive brittle failure if the strain rate increases further.

In order to use results from naturally reequilibrated fluid inclusions to infer P-T histories, it is necessary to understand the mechanisms of stretching and decrepitation of fluid inclusions, and how these mechanisms operate to affect inclusion density and composition. If the inclusions fail in a brittle manner, then one should observe dry fractures around the fluid inclusions. If, however, the crystal surrounding inclusions in quartz behaves plastically, then one should observe a high density of dislocations in glide and/or climb configuration around fluid inclusions, as well as precipitation of water in the form of tiny bubbles. Among the first workers to recognize the important role of dislocations in the reequilibration of fluid inclusions were Wilkins et al. (1981), Bodnar and Bethke (1984), Sterner and Bodnar (1986), Sterner et al. (1988), Boullier et al. (1989), Bakker and Jansen (1990) and Hollister (1990). To understand better the mechanisms operating during inclusion deformation, we have conducted a detailed TEM study of the lattice defects around reequilibrated aqueous synthetic inclusions in natural Brazilian quartz,

building upon results from earlier studies (cf., Bakker and Jansen 1994). The goal of this study is further to develop our understanding of the processes involved in deformation of quartz surrounding fluid inclusions. This will allow us better to predict the deformational history of fluid inclusions deformed in nature, based on observations of the microstructural features in the quartz host.

Experimental details

Three samples previously studied by Vityk and Bodnar (1998) to monitor density changes of synthetic fluid inclusions during decompression were used in the present work for microstructural observations. Synthetic 10 wt% NaCl fluid inclusions were trapped at 700 °C and 5 kbar (Fig. 2, inset) in three separate pressure vessels by healing fractures in Brazilian quartz (Bodnar and Sterner 1987). Formation conditions were close to the quartz α/β transition but within the α-quartz field, based on the absence of Daupiné twinning in the quartz in healed fractures. After formation, one vessel was quenched isochorically. This sample (ITD-0) was used for TEM characterization of preexisting (i.e., formed during the fracture healing process) microstructures around the undeformed synthetic fluid inclusions. The remaining two vessels were decompressed over a period of a few hours along a nearly isothermal *P-T* path (Fig. 2, inset) to simulate retrograde *P-T* conditions in high-grade metamorphic environments (for experimental details see Vityk and Bodnar 1995a). Final conditions (625 °C and 2 kbar) resulted in a cumulative internal overpressure ($P_{internal} - P_{confining}$) of about 2.1 kbar. At these final conditions, samples were held for 30 days (sample ITD-3-30) or 180 days (sample ITD-3-180).

After the experiments, each sample was wafered into 1 mm thick disks and polished to identify regions with abundant fluid inclusions. The disks were thinned to 30 μm, then polished with CeO_2. Final thinning to electron transparency was achieved by ion-thinning (Ar, 5 kV, 15 °C). During this final procedure, each disk was positioned such that the "inclusion-rich" portion of the disk would be located within the electron transparent edge of the thin foil after thinning. The defect microstructures were imaged using a Philips CM30 TEM in the "two beam condition", which allows an unambiguous characterization of lattice defects. In practice, the thin foil is tilted in the electron microscope until only one family of lattice planes is at Bragg conditions. The best families of reflecting planes in quartz are the rhombohedral planes {1 0 1 1} which present the largest structure factor, i.e., the brightest images at a given electron beam density, and thus require the shortest exposure under the electron beam to obtain a usable image. This is an important experimental condition because quartz is very sensitive to electron beam irradiation and becomes damaged within seconds with a high intensity beam. With a moderate intensity beam very tiny irradiation defects (dark contrasts) nucleate within minutes and can be confused with tiny water bubbles.

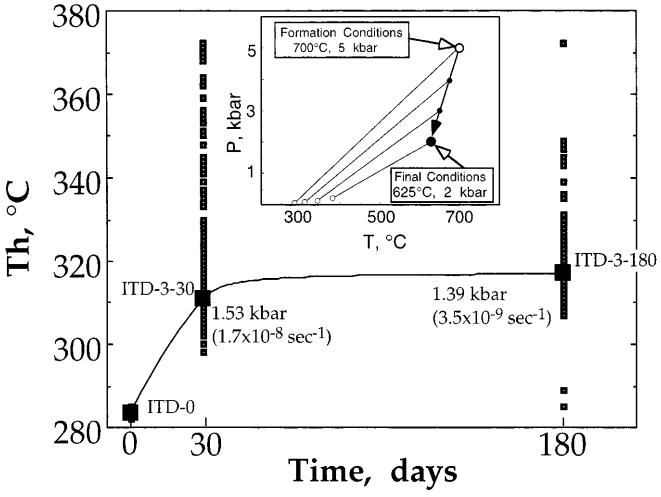

Fig. 2 Evolution of the mean homogenization temperatures (*large squares*) calculated for measured *T*hs (*small squares*) of synthetic inclusions in samples reequilibrated for 0 days (ITD-0), 30 days (ITD-3-30), and 180 days (ITD-3-180) plotted as a function of the duration of the experiments. The pressures (in kbar) *adjacent to the large squares* are the average final internal pressures during reequilibration, calculated from the mean *T*h values (see Vityk and Bodnar 1998, for details). The *numbers shown in parenthesis* underneath the internal pressures are inclusion deformation strain rates. *Inset* shows the *P-T* path simulating nearly isothermal decompression during reequilibration. The *large, open circle* shows the *P-T* conditions of inclusion formation (700 °C, 5 kbar), and the *large filled circle* represents the final reequilibration conditions (625 °C, 2 kbar). The *small filled circles* along the decompression path represent *P-T* conditions where the samples were held for 7 days during each stage of decompression. The *small open circles* represent *P-T* points along the liquid-vapor curve for 10 wt% NaCl-H_2O corresponding to iso-*T*h lines (*light lines*) for *P-T* points along the decompression path. The iso-*T*h lines for 10 wt% NaCl-H_2O solution were calculated using the equation of state of Bodnar and Vityk (1994)

Microstructural observations

Microstructures developed during initial inclusion trapping

To characterize microstructures developed during original formation of synthetic fluid inclusions (sample ITD-0), we compared the microstructural features of quartz at some distance from fluid inclusions with those of quartz in the immediate vicinity of inclusions. It should be noted that TEM images are 2-dimensional and it is not possible to determine if there were previously inclusions below or above the area that was analyzed. However, the rarity of inclusions at the scale of the TEM images, combined with the uniformity of features among the several inclusions examined, suggests that the features we describe are associated with the inclusions observed in the TEM images. The host quartz far away from fluid inclusions shows an almost perfect crystal with rare dislocations associated with the fracture plane. Areas surrounding fluid inclusions, however, show a fairly high density of dislocations, consisting of dislocation loops which appear to have been preferentially activated on one side of the fluid inclusions (Fig. 3A, B). These dislocations are restricted to narrow bands along (or in the vicinity of) healed fracture surfaces. In places, the dislocations are accompanied by rare clusters of tiny strain-free bubbles of water with a weak brightness contrast arising mostly from differences in absorption. Some other large water bubbles are clearly visible owing to their strain contrasts (i.e., the two dark lobes separated by a line-of-no-contrast in Fig. 3C). Note that most of these tiny bubbles are connected to dislocation lines. The fact that most bubbles are aligned along dis-

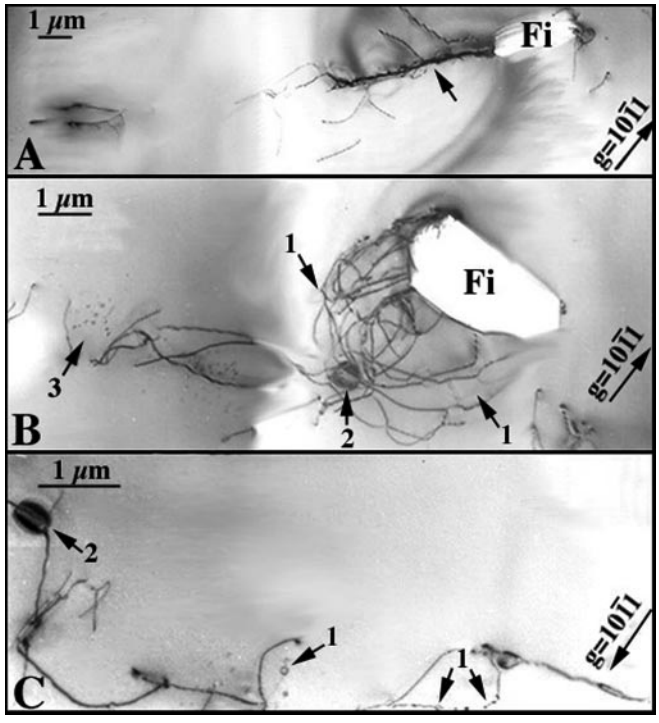

Fig. 3A–C A sequence of TEM photomicrographs illustrating typical microstructures associated with fluid inclusions produced during healing of microfractures at 700 °C and 5 kbar. **A** Set of dislocations (*arrow*) that has been preferentially activated on one side of a fluid inclusion. **B** Dislocation loops nucleated on the walls of a synthetic inclusion are indicated by the *arrows labeled 1*. *Arrow 2* shows a small water bubble surrounded by a strain field (*dark zones*); *arrow 3* highlights an area with tiny strain-free bubbles. **C** Two different types of grown-in bubbles associated with fracture dislocations: strain-free bubbles isolated and attached to dislocations (*arrows 1*), and bubbles showing a line-of-no-contrast reflecting strain of the matrix (*arrow 2*)

locations strongly suggests that the dislocations nucleated first and then the bubbles preferentially nucleated on the dislocations.

Dislocation microstructures in the immediate vicinity of the fluid inclusion walls, but outside of the fracture plane, are shown in Fig. 4. The original fracture plane can be identified because the lattice planes on either side of the fracture do not match up perfectly, resulting in generation of dislocations where they intersect. The dislocation density outside of the fracture plane is much lower compared to areas adjacent to fluid inclusions and within the fracture plane. Some inclusions also show dislocations attached to the corners of the inclusion walls (Fig. 4A). Dislocation activity outside of the fracture plane is restricted to the area immediately surrounding the inclusions. Water bubbles were not detected within cores of dislocations or in the vicinity of dislocations outside of the fracture plane. Overall, the dislocation activity is lower around smaller fluid inclusions, and higher around larger inclusions, as illustrated in Fig. 4B. The area around the small fluid inclusion is practically free of defects (only one dislocation on its right side), whereas the larger inclusion is surrounded by a number of dislocations extending 1 to 2 μm from the inclusion walls.

Microstructures developed during the 30 day reequilibration experiment

Synthetic fluid inclusions reequilibrated at 650 °C and 2 kbar under conditions of internal overpressure for 30 days are surrounded by defect microstructures markedly different from those in the un-reequilibrated sample ITD-0, as shown on Figs. 5–7. For some inclusions the highest dislocation and water bubble density is observed within narrow zones connected to the inclusion walls (Fig. 5A, B). This high density of defects outlines the healed fracture. Other inclusions, however, show only a few dislocation segments which do not extend far from the inclusion wall (Fig. 6A, B). Clearly plastic deformation was not activated around these latter inclusions.

Still other inclusions, like the one shown in Fig. 7, display a high activity of dislocations. The dislocation

Fig. 4A, B TEM photomicrographs showing dislocation structures generated during original formation of fluid inclusions at 700 °C and 5 kbar. **A** Photomicrograph of a negative crystal-shaped fluid inclusion with low dislocation density and no bubbles. Note that the dislocation activity is restricted to the immediate vicinity (≤1 μm) of the inclusion walls. **B** Photomicrograph illustrating the effect of inclusion size on the activity of dislocations around synthetic fluid inclusions. Note that the smaller inclusion is practically free of lattice defects. The larger inclusion, however, is surrounded by lattice defects

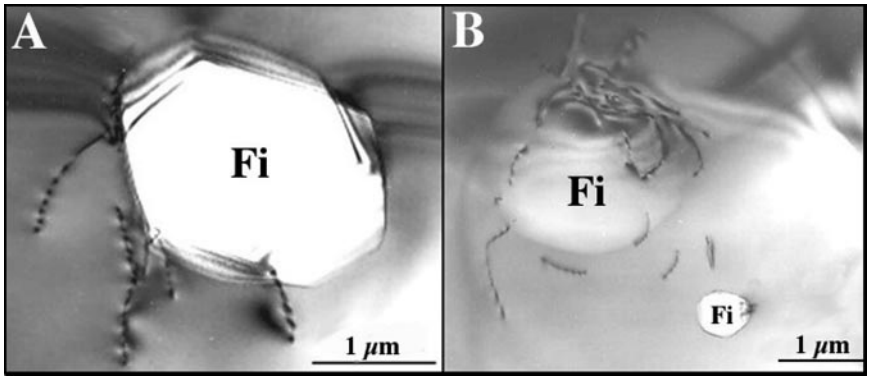

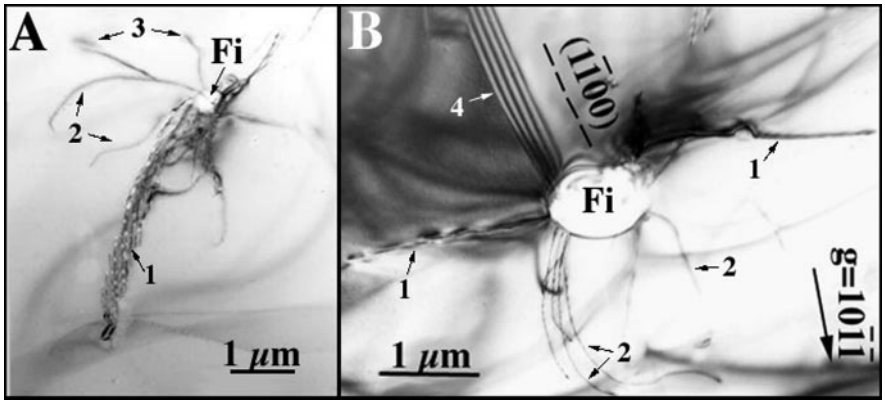

Fig. 5A, B TEM photomicrographs showing microstructures produced during the 30 day reequilibration experiment at 625 °C and 2 kbar. **A, B** Fluid inclusions are surrounded by poorly healed fractures (*arrow 1*), a few dislocations connected to the inclusion walls (*arrows labeled 2*), and a Dauphine twin (*arrow #4* in B). Note the high density of water bubbles in the healed fracture in **A**. Also note that some dislocations are pinned with bubbles (*arrows #3* in **A**)

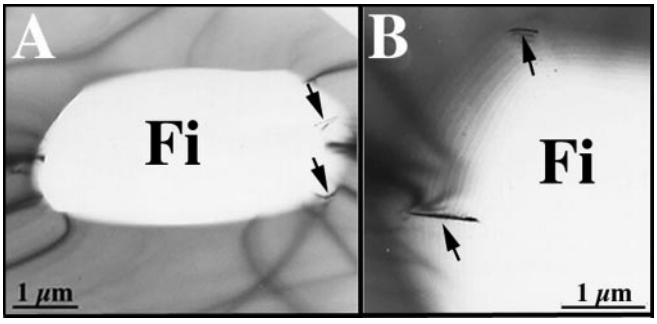

Fig. 6 TEM photomicrographs showing microstructures associated with a fluid inclusion after reequilibration for 30 days at 625 °C and 2 kbar. Note the two dislocations on the fluid inclusion walls (**A**). An enlargement of similar dislocations is shown in (**B**)

activity is observed in two different settings, referred to here as zone 1 and zone 2. Dislocation activity in zone 1 extends over 15 μm from the fluid inclusion walls. Most dislocations are *a* dislocations in glide configuration in rhombohedral planes (glide systems $(1\,0\,1\,1)\frac{1}{3}[1\,2\,1\,0]$), and are preferentially activated at the corners of the inclusion walls (Fig. 7A, arrow). Many dislocations have crystallographically controlled orientations (Fig. 7D). Water bubbles, either strain-free or with a characteristic strain-field contrast, are also common. Bubble activity extends over 7 μm from the inclusion shown in Fig. 7A.

Most of the dislocations in zone 2 lie in the (1 0 1 1) plane of the thin foil and are out of contrast with the diffraction vector $g = 1011$. These dislocations have a Burger vector $b = \frac{1}{3}[1\,2\,1\,0] = a_2$. The glide system $(1\,0\,1\,1)\frac{1}{3}[1\,2\,1\,0]$ was thus activated during deformation. Tiny strain-free water bubbles are common in zone 2. Many water bubbles pin dislocations (or were nucleated on the dislocations) (Fig. 7B, C).

Microstructures developed during the 180 day reequilibration experiment

A large area of quartz containing two fluid inclusions reequilibrated for 180 days is shown in Fig. 8. Dislocation activity occurs in narrow band-like regions which are thought to represent healed fracture zones between the fluid inclusions. These dislocations are pinned by water bubbles exhibiting a strong strain field (''coffee bean contrast'') (Fig. 9A). These bubbles were also observed in the 30 day experiment, mostly in healed fracture zones, but single bubbles or small clusters of bubbles were also detected far from the healed fracture surface. Bubbles exhibiting the ''coffee bean contrast'' rarely occur more than a few micrometers away from inclusions. Many tiny strain-free bubbles, both isolated and along dislocations, were observed in the sample reequilibrated for 180 days (Figs. 8, 9B and 10). The largest concentration of these bubbles was observed in healed fractures, where they show a mean spacing of approximately 700 Å and often pin dislocations (Fig. 10B). The scalloped texture of the dislocation lines indicates that the dislocations are strongly pinned and unable to break free of the bubbles and migrate through the quartz. The portion of the dislocation between two pinning points was able to migrate some small distance in response to the applied stress, but, the stress was not large enough to allow the dislocations to become unpinned and escape (Fig. 10B). In regions away from fluid inclusions, where the bubble concentration is considerably lower, some dislocations were able to unpin and move (glide) over distances of several micrometers. Figure 11A illustrates some of the different types of interactions between strain-free bubbles and dislocations in a region close to the healed fracture zone. Clearly, some bubbles formed early and then pinned the later mobile dislocations (as indicated by the orientations of the cusps along dislocation lines).

Dislocation glide was also detected in the vicinity of the fluid inclusion walls but outside of the fracture plane, in regions with relatively low concentrations of strain-free bubbles (Fig. 12). Some bubbles show a spherical shape, whereas others are fully relaxed and elongated in the $c = [0\,0\,0\,1]$ direction (Fig. 9B). Overall, dislocations in glide configuration have preferential directions, parallel to [0 0 0 1] and [1 2 1 0] (Fig. 12B, C).

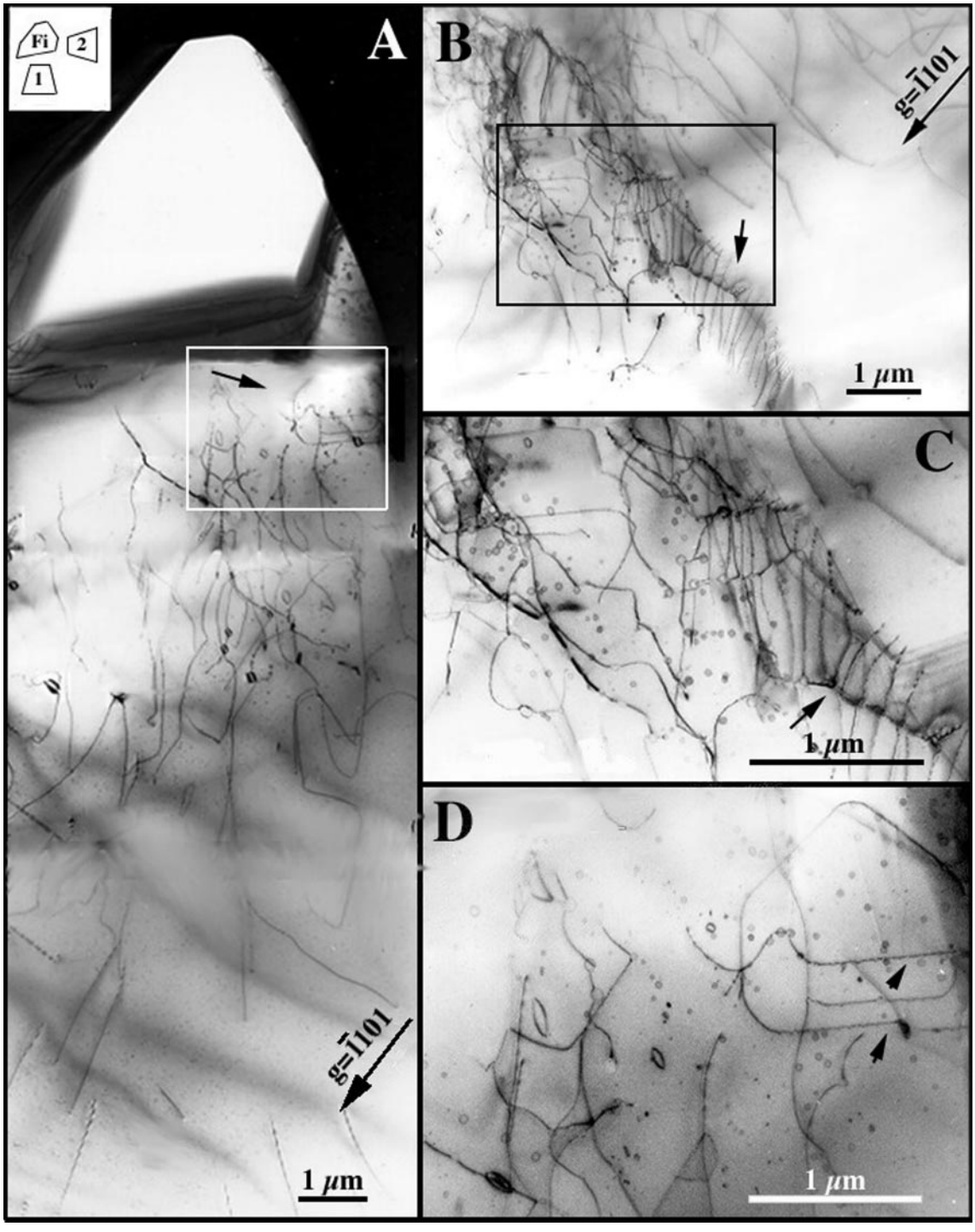

Fig. 7A–D A sequence of TEM photomicrographs showing dislocation microstructures around a fluid inclusion that was reequilibrated for 30 days at 625 °C and 2 kbar. The dislocation microstructures were observed in two directions (see schematic drawing in *upper left corner* of **A**). **A** Represents zone 1; note that there is almost no dislocation activity in the immediate vicinity of the fluid inclusion. Dislocation activity extends greater than 15 μm from the inclusion (beyond the field of view of the photomicrograph). Bubble activity extends more than 7 μm from the inclusion. Most of the dislocations observed are a_2 dislocations belonging to the glide system (1 0 1 1)1/3[1 2 1 0]. **B**, **C** Show microstructures in zone 2 (see drawing in **A**). Most dislocations are in the plane of the thin foil (1 0 1 1), with a Burgers vector of $\frac{1}{3}$[1 2 1 0] = a_2. Note the large density of closely spaced en-echelon-like dislocations (*arrow* in **B**). Also note the tiny strain-free bubbles. **D** Is an enlargement of the portion of zone 1 shown in **A**. Some dislocations show preferred crystallographic orientation (*arrows*)

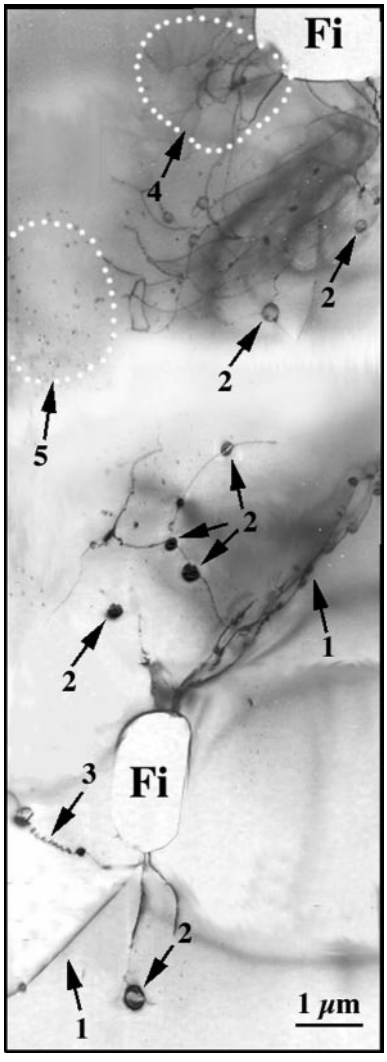

Fig. 8 TEM photomicrograph of microstructures around fluid inclusions after reequilibration for 180 days at 625 °C and 2 kbar. Note the long segments of dislocations attached to the fluid inclusion walls (*arrows #1*). These dislocations are pinned with "strained" bubbles (*arrows #2*) and strain-free bubbles (*arrow #3*). *Arrow 4* highlights the region with a high density of dislocations which are gliding away from a fluid inclusion. *Arrow 5* highlights the area with spots of irradiation damage in the TEM

Discussion

In the following discussion, fluid inclusion reequilibration observed in this study is interpreted to be the product of two separate but related processes. The first process involves activity of dislocations in the "wet" quartz filling the original fracture, with no loss of fluid from the inclusion – this process is referred to as stretching. The second process involves loss of water from the inclusion along these same dislocations as well as along new dislocations generated during the reequilibration process. This process is referred to as leakage. In practice, these two processes are probably complementary and operate in parallel, but for the sake of simplicity they are discussed separately below.

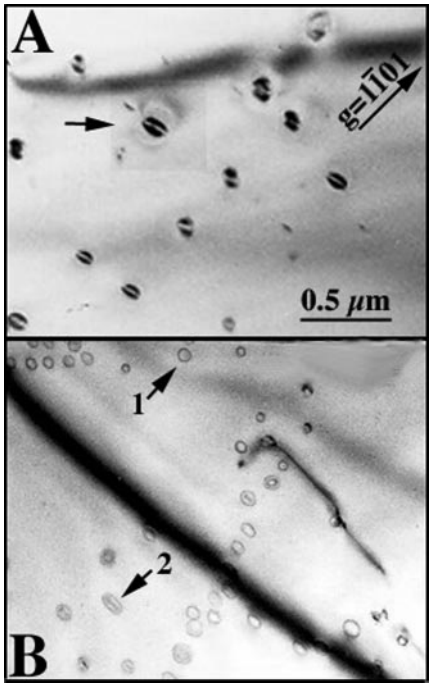

Fig. 9 TEM photomicrographs showing two different types of water bubbles observed around fluid inclusions after reequilibration for 180 days at 625 °C and 2 kbar. Water bubbles with a line-of-no-contrast, reflecting strain of the matrix, are indicated by the *arrow* (**A**). Strain-free, approximately circular bubbles, (*arrow #1*) and crystallographically shaped bubbles (*arrow #2*) are shown (**B**)

Quartz flow by stretching

Our TEM observations indicate that reequilibrated inclusions are surrounded by dislocations and tiny bubbles of water. Bakker and Jansen (1990, 1991) observed similar features associated with laboratory-reequilibrated fluid inclusions in quartz. Two types of dislocation activity are associated with reequilibrated inclusions. The first type is represented by dislocation entanglements often located between adjacent fluid inclusions (e.g., Figs. 8, 10 and 12). Similar dislocations were observed around fluid inclusions before reequilibration (Fig. 3), thus we conclude that these dislocations are related to the original fracture healing process. These dislocations occur in quartz that was precipitated during the fracture healing process – they are referred to hereafter as *fracture dislocations*. The TEM observations of areas close to the healed fractures before and after reequilibration show that these regions contain numerous bubbles imaged by a characteristic strain field, indicative of high internal pressure at room temperature. Similar "strained" water bubbles were reported by McLaren et al. (1983, 1989) and Gerretsen et al. (1989) for "wet" (up to $1600H/10^6Si$) synthetic quartz crystals. Following the suggestions of these previous workers, these bubbles are interpreted as high pressure clusters of molecular water formed during precipitation of "wet" quartz in the fracture plane. Other, tiny strain-free bubbles occur both isolated and on fracture dislocations.

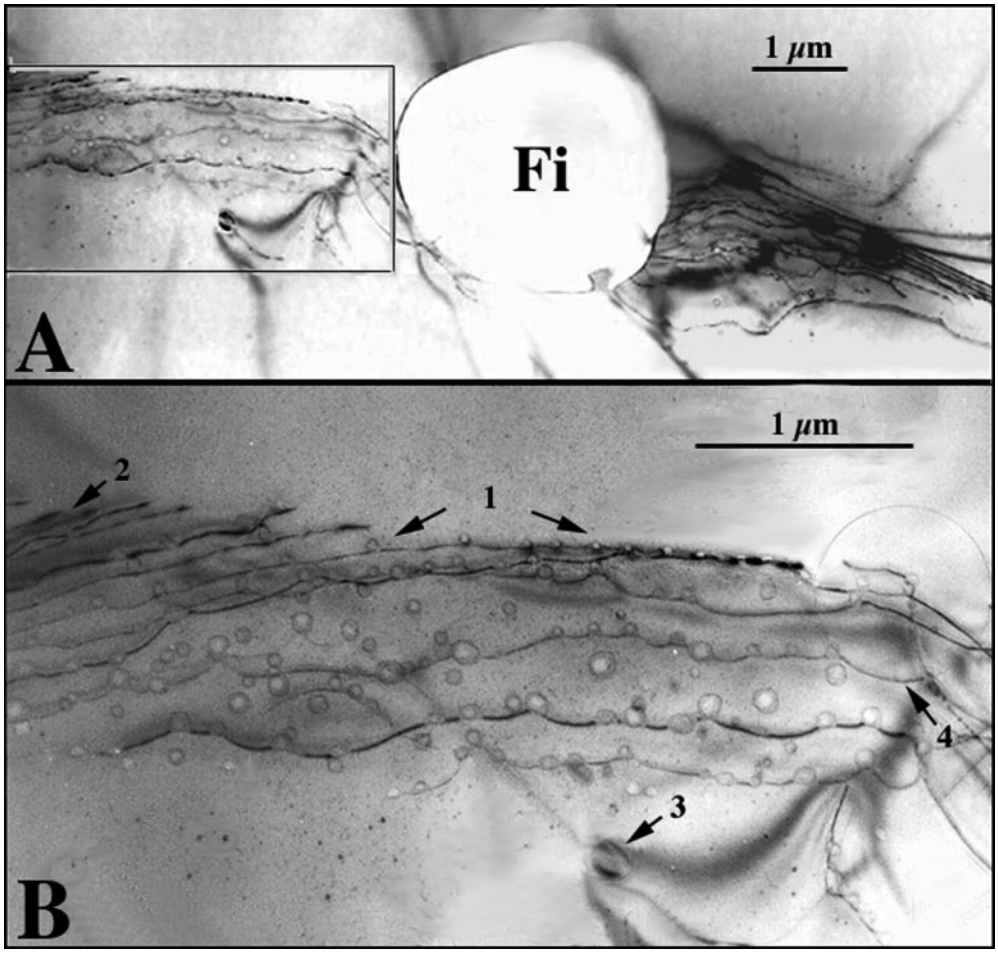

Fig. 10A, B TEM photomicrographs of dislocation microstructures after reequilibration for 180 days at 625 °C and 2 kbar: **A** Shows the healed fracture region adjacent to a fluid inclusion; **B** is an enlargement of the area indicated by the *rectangle* in **A**. Note that the dislocations are pinned with strain-free bubbles. *Arrow #1* in **B** highlights a dislocation pinned with small, closely spaced, strain-free bubbles (1 bubble every 600 to 800 Å). The spacing of the bubbles increases away from the fluid inclusion. *Arrow 2* indicates the area with the lowest concentration of strain-free water bubbles. This area contains dislocations that do not appear to be connected to the fluid inclusion. *Arrow 3* highlights a bubble with a contrast due to its stain field. Note the "scalloped" configuration of many fracture dislocations (e.g., *arrow 4*)

These bubbles are interpreted to represent precipitation of (4H)Si defects (Kronenberg 1994; Cordier and Doukhan 1989).

After reequilibration, healed fractures reveal dramatic modifications of their microstructures (Fig. 10), compared to un-reequilibrated material. After equilibration, a majority of the fracture dislocations became pinned by strain-free water bubbles. In places, these dislocations show a "scalloped" configuration, which indicates that these dislocations were subjected to high differential stress, but were not able to unpin from the bubbles (Fig. 10B). This suggests a restricted mobility of fracture dislocations connected to fluid inclusions, and thus a limited plasticity of the inclusion walls adjacent to the healed fracture plane. However, dislocation glide is observed in the matrix over distances up to 12 μm away from the fluid inclusions. In this "remote" fracture area, the concentration of water bubbles is considerably lower than in the immediate vicinity of the inclusion, and the dislocations in this area were able to unpin and glide up to a few micrometers away from the fracture plane.

The mobility of fracture dislocations contrasts with dislocations from areas outside the fracture plane, where they are not damped by water bubbles and can glide more freely. In both the 30 and 180 day experiments, dislocations appear to have glided away from fluid inclusions in the rhombohedral planes {1 0 1 1} (Figs. 7 and 12). Most of the dislocations have a Burger vector $b = \frac{1}{3}(1\ 2\ 1\ 0)$. The dislocations were created during original formation of the fluid inclusions during fracture healing (see e.g., Fig. 4), and then, under stress, migrated a few microns away from the fluid inclusions. Some dislocations, however, might have nucleated on the inclusion walls during reequilibration in response to local stress concentrations. Often, these dislocations appear to be "chained" to the inclusion walls by tiny water bubbles which limit their mobility (Fig. 12A). In the following discussion these dislocations are referred to as *wall dislocations*. In some places (with lower bubble concentrations?), the wall dislocations bow out, become unchained from the inclusion walls, and glide away to become active sites for further dislocation multiplication through a mechanism such as the Frank-Read Source.

Climb microstructures were only observed around fluid inclusions that were reequilibrated for 180 days (ITD-3-180 sample, Fig. 11A, B). Climb appears to have been active in the healed fracture area around fluid inclusions (Fig. 11A), where fracture dislocations are pinned by bubbles. Climb also occurred in the quartz matrix up to 10 μm away from the fracture plane. During climb, dislocations are able to navigate around obstacles such as bubbles. Thus, it becomes easier to

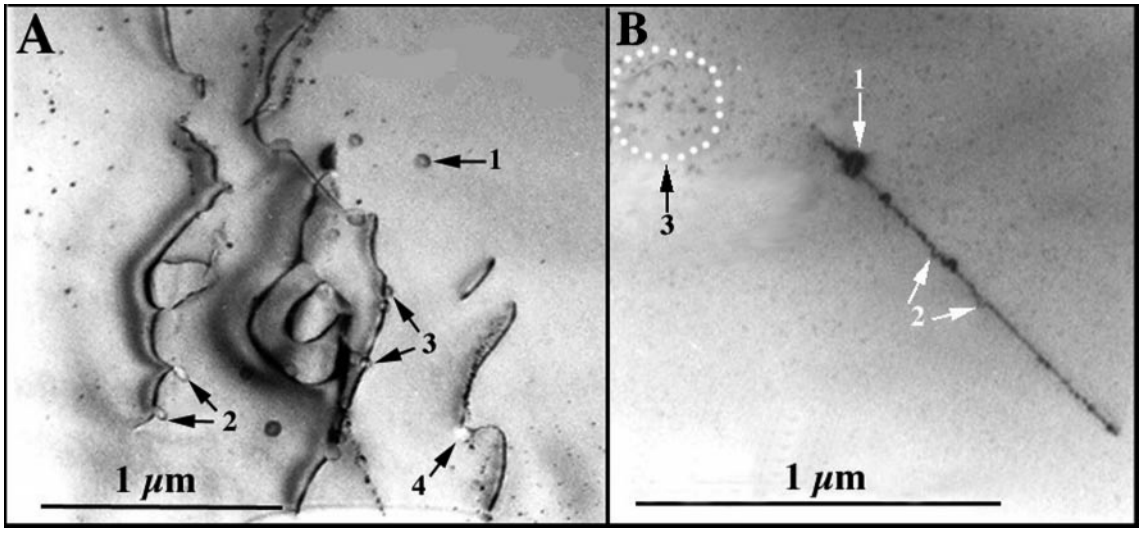

Fig. 11A, B TEM photomicrographs showing microstructures associated with dislocation climb. These microstructures were produced during the 180 day experiment at 625 °C and 2 kbar. **A** illustrates some of the different types of interactions between bubbles and dislocations. Some bubbles appear to be isolated from the dislocations (*arrow #1*). Some early formed bubbles were later pinned by the mobile dislocation (*arrow #2*). Some bubbles were nucleated on the dislocations (*arrow #3*). Bubble growth was also assisted by dislocation climb (*arrow #4*). **B** Shows another example of a dislocation which has been pinned with a water bubble. The bubble shows a strain contrast (*arrow #1*). Note the dislocation zig-zag in some places (*arrows #2*), which is indicative of climb. *Arrow #3* highlights an area with *dark spots* of irradiation damage

deform a crystal at a low strain rate where solid-state diffusion processes become more important. After the 30- and 180-day experiments, synthetic fluid inclusions show a decrease in fluid density, which can be related to flow of the inclusion walls under differential pressure. Inclusion flow results in a permanent increase in inclusion volume (defined as ''inclusion strain'' by Vityk and Bodnar 1998). The increase in the inclusion strain reduces the internal pressure of the fluid inclusion, shifting (reducing) inclusion density towards the final reequilibration isochore. The average inclusion strain rate, however, was considerably higher for inclusions during the 30 day experiment than during the 180 day experiment (Fig. 2). During the 30 day experiment, recovery from high internal stresses was a relatively rapid process (Fig. 2), and this rapid recovery at the early stages of

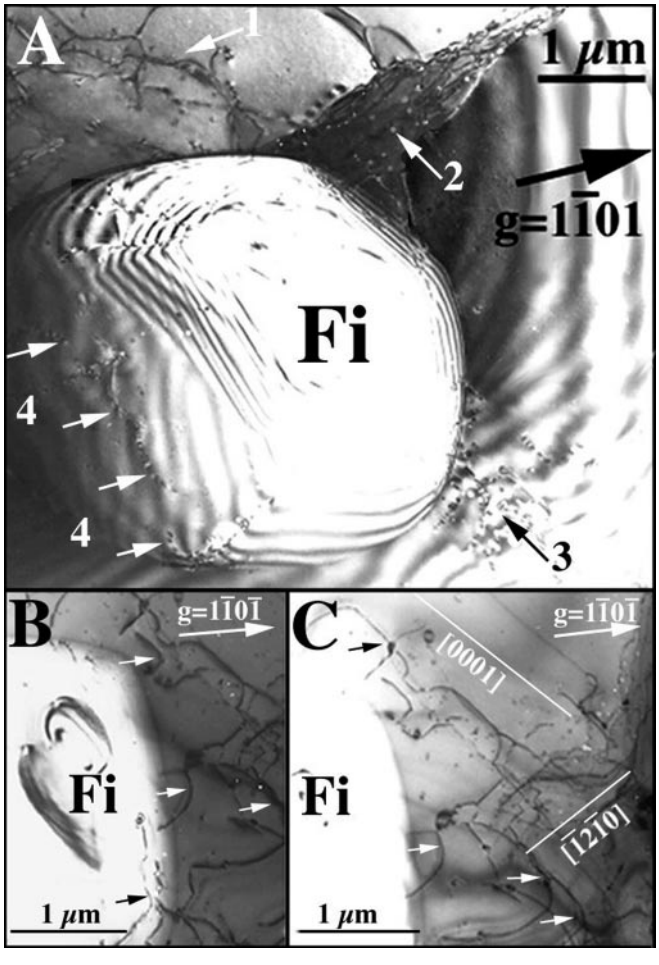

Fig. 12A–C Dislocation structures at and near fluid inclusions produced during 180 days reequilibration at 625 °C and 2 kbar. The *wavy thick lines* with a weak contrast are contours of equal thickness, reflecting the fact that the observed area is not a perfect plane. This results either from irregular ion thinning or from imperfect mechanical polishing. **A** *Arrows* indicate a typical set of microstructures which developed around a synthetic fluid inclusion (*Fi*) during the experiment: *arrow 1* shows mobile dislocations gliding away from the fluid inclusion; *arrow 2* shows dislocations pinned by strain-free water bubbles in the healed fracture area; *arrow 3* shows the area with high density of tiny strain-free bubbles nucleated in the vicinity of the fluid inclusion; *arrows 4* show a series of ''chain-like'' structures nucleated on the inclusion walls. These structures consist of dislocation segments (wall dislocations) tightly pinned with strain-free water bubbles. **B** and **C** *Arrows* highlight ''ripples'' of dislocations gliding away from a fluid inclusion under the action of differential stress. The dislocations on the inclusion surface (*black arrow* on **B**) are pinned by bubbles. Many dislocations exhibit preferred orientation parallel to **c** and **a** typical of glide configuration. Some dislocation loops are bowed out in the (1 0 1 0) glide plane and show straight segments parallel to [0 0 0 1] (lowest mobility)

inclusion deformation was controlled by dislocation glide and water diffusion. Over the next 150 days (in the 180 day experiment) continued recovery was very slow (Fig. 2), suggesting that inclusion internal overpressure was reduced such that the imposed high strain rate observed in the first 30 days could not be maintained. Under conditions of low strain rate in the 180 day experiment, deformation of fluid inclusions was controlled by a combination of dislocation glide and climb.

The mobile dislocations in glide and climb configuration are referred to as *strain-induced dislocations*. It is suggested that during earlier stages of loading (high overpressure and high strain rate), fluid inclusion deformation is glide-controlled. Dislocations are commonly developed in zones surrounding fluid inclusions to relieve stresses on the inclusion walls. During the later stages of loading (low overpressure and strain rate), deformation is controlled by both glide and climb, with the assistance of water. The inclusion walls are weakened by water that diffuses from the inclusions into the surrounding quartz. Our TEM observations confirm the presence of water around fluid inclusions in the form of strain-free bubbles that are often associated with strain-induced dislocations (Figs. 7, 11 and 12). In general, glide and climb activity are observed in the immediate vicinity of the fluid inclusions (< 3 μm), suggesting that plasticity was restricted to narrow crystallographically oriented zones within the otherwise undeformed inclusion walls. However, tangles of long dislocation segments, which extend over 15 μm away from the inclusion walls, are also observed.

The density of strain-induced dislocations varies considerably from one inclusion to the next in the sample from the 30 day experiment, suggesting that the response of the fluid inclusions to an imposed stress was extremely variable. This suggests an original mechanical heterogeneity for the inclusions. The TEM observations of undeformed material showed that large fluid inclusions generally display a relatively high activity of dislocations, whereas small inclusions often lack associated dislocations. This observation is consistent with results of earlier studies which show a close relationship between inclusion size and the ease with which a fluid inclusion reequilibrates (Leroy 1979; Ulrich and Bodnar 1988; Bodnar et al. 1989). It should be noted that the shape and local stress distribution around the inclusion walls can also affect the deformability of fluid inclusions.

Leakage of water from inclusions via diffusion

Earlier workers have described the application of microthermometry and TEM analysis to document post-entrapment leakage of synthetic fluid inclusions. Hall and Sterner (1993) suggested that preferential leakage of water from synthetic fluid inclusions occurred by selective diffusion of water along dislocations (dislocation-induced leakage), resulting in an increase in inclusion salinity. This conclusion is consistent with TEM observations of Bakker and Jansen (1994), who reported newly formed, strain-free water bubbles on dislocation lines around synthetic fluid inclusions. These water bubbles were thought to represent water that escaped from the fluid inclusions.

Our TEM observations reveal the presence of preexisting dislocations around synthetic fluid inclusions formed at 700 °C and 5 kbar. Most of the preexisting dislocations occur in the area corresponding to the healed fracture. Before reequilibration, only a few strain-free water bubbles were associated with these dislocations. After reequilibration, the dislocations were found to be heavily decorated by strain-free bubbles (Fig. 10). How did these bubbles develop? First, there must be a source of water. Second, there must be a mechanism for nucleation of the bubbles. As shown in Fig. 10B, strain-free bubbles nucleated mostly on dislocations that are directly connected to fluid inclusions. Dislocations not connected to fluid inclusions carry very few or no water bubbles. The concentration and size of the bubbles also decrease away from the inclusion. Together, these observations suggest that water leaked from overpressured inclusions along dislocation lines connected to the inclusion walls (pipe diffusion). A drop in confining P during decompression enhanced the precipitation of bubbles.

As was suggested by many previous workers (Kerrich 1976; Wilkins and Barkas 1978; Boullier et al. 1989; Hollister 1990; Bakker and Jansen 1991; Cordier et al. 1994), preferential leakage can occur as a result of plastic deformation of fluid inclusions (strain-enhanced leakage). During plastic deformation, water can be extracted from a fluid inclusion by strain-induced mobile dislocations. Our TEM observations confirm the presence of strain-induced dislocation loops attached to the walls of reequilibrated fluid inclusions. Our observations also show the presence of water in the form of strain-free isolated bubbles and bubbles connected to dislocations. Both spherical bubbles and bubbles elongated in the $c = [0\ 0\ 0\ 1]$ direction are observed (Fig. 9). The different shapes of the bubbles are indicative of their different annealing times. There was continuous nucleation of bubbles in the immediate vicinity of the fluid inclusions during the experiments, suggesting a continuous water supply. Quartz in this area was wet, with a large concentration of (4H)Si defects, arising either from bulk water diffusion from a fluid inclusion into the quartz matrix, or from pipe diffusion along preexisting dislocations on the inclusion walls. Further bubble growth was enhanced by strain-induced dislocations, owing to rapid pipe diffusion of the (4H)Si defects being swept along by the mobile dislocations in their glide planes (Doukhan and Trepied 1985).

Our TEM observations show no evidence of precipitation of wet quartz outside of the fracture plane. However, TEM analysis revealed a 1–3 μm plastic zone around experimentally reequilibrated fluid inclusions. Because dry Brazilian quartz used in our experiments is virtually undeformable (Griggs and Blacic 1964, 1965),

we conclude that water diffusion must be involved in the reequilibration of fluid inclusions under conditions of internal overpressure, and that water assists plasticity of the host via hydrolytic weakening.

According to Cordier et al. (1994), pipe diffusion via pinned fracture dislocations, as well as water removal by strain-induced mobile dislocations, has a negligible effect on kinetics of water leakage because of the low water storage capacity of these dislocations (a dislocation line can store a maximum of one water molecule per 5 Å of length) and the relatively low number of dislocations connected to each fluid inclusion. Our microstructural observations show, however, a considerable variation in the number of dislocations connected to fluid inclusions and in the density of strain-free bubbles on these dislocations (compare, for example, an inclusion in Fig. 8 and the inclusion in Fig. 10A). This suggests that the amount of water that might be lost from individual fluid inclusions via dislocations depends on many factors, including original water saturation of the dislocations, the density of dislocations, local stress concentrations, etc.

The maximum amount of water that could have been lost from low salinity synthetic inclusions along dislocations can be measured microthermometrically by comparing compositions of fluid inclusions before and after reequilibration (see also Sterner and Bodnar 1989; Hall and Sterner 1993). For example, after the 180 day experiment, a large percentage of inclusions (about 40%) showed a small decrease in the melting temperature of ice, from the original −6.6 °C to −6.8 °C (Fig. 13). This decrease in Tm corresponds to an increase in salinity from 10.0 to 10.2 wt% NaCl-H_2O. The observed increase in salinity (0.2 wt% NaCl) is greater than the precision of salinity determinations (approximately 0.1 wt% NaCl), and can be explained by preferential loss of water from the inclusions. The observed salinity change also constrains the maximum amount of water that could have been lost. Thus, Fig. 13 shows the salinity (10.6 wt% NaCl) required to account for the density change observed in the 180 day experiments (assuming that the volume remains constant). The observed salinity change (0.2 wt% NaCl) is less than the predicted change (0.6 wt% NaCl), and thus too small to account for the total density change, suggesting that the process responsible for the decrease in inclusion density includes *both* water loss and plastic volume change. Volumetric calculations indicate that the total density change that occurred during reequilibration is about 5 percent. This assumes that the inclusion composition remained constant during reequilibration (i.e., nothing is added to or lost from the inclusion). About 40 percent of the total observed density change can be attributed to preferential water loss by the fluid inclusions. The remaining 60% of the density change is attributed to inclusion strain (volume change) resulting from stretching.

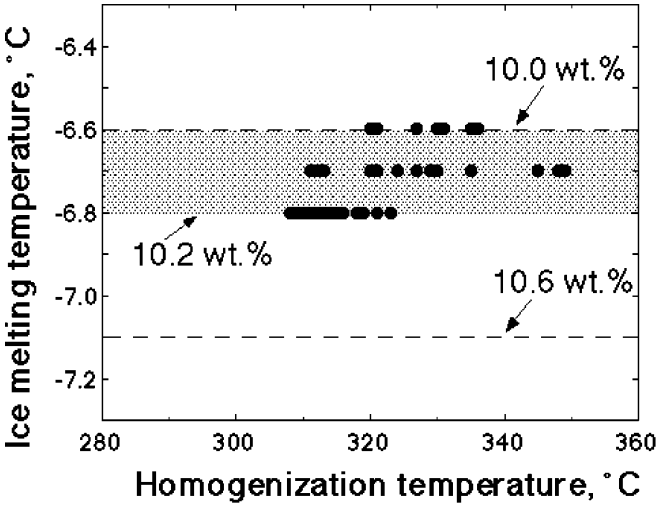

Fig. 13 Variation of ice-melting temperatures for fluid inclusions reequilibrated for 180 days. The original salinity of the synthetic fluid inclusions was 10 wt% NaCl. The maximum salinity observed for the inclusions after reequilibration was 10.2 wt% NaCl. Inclusion salinity required in order to account completely for the observed *T*h change by leakage of water is 10.6 wt% NaCl. Salinities were calculated using the equation of Bodnar (1993)

Summary

Quartz in the vicinity of healed fractures in un-reequilibrated samples shows a moderate to high dislocation density. Reequilibration generates a progressive increase in dislocation density in regions outside of the fracture plane, as well as continuous water precipitation in the form of strain-free bubbles around fluid inclusions. Water bubbles in the fracture nucleate and grow by pipe diffusion of water from the inclusions via preexisting inherited dislocations. Water bubbles outside of the fracture plane originate via strain-induced water loss along mobile dislocations. Most mobile dislocations nucleate at inclusion walls (*wall dislocations*). The larger the inclusion, the higher the dislocation activity, suggesting a size-dependent deformation behavior for the fluid inclusions, at least during the earlier stages of deformation. This conclusion is consistent with earlier work by Bodnar and Bethke (1984) and Vityk and Bodnar (1998).

The increase in dislocation density around fluid inclusions and the concomitant decrease in fluid density of the inclusions (from 0.84 to 0.79 g/cc) are both a result of flow of the inclusion by stretching. The amount of stretching produced during the 180 day experiment corresponds to about a 3% increase in inclusion volume (inclusion strain). Stretching of the inclusion walls occurred anisotropically by expansion of mobile dislocations in their slip systems. Dislocation expansion was controlled by glide in the rhombohedral planes {1 0 1 1} and was restricted to narrow zones (≤3 μm) in the immediate vicinity of the fluid inclusion walls outside of the healed fracture plane. These plastic zones were observed after both short term (30 days) and long term (180 days) experiments and are attributed to hydrolytic weakening

of the quartz matrix around fluid inclusions owing to water diffusion into the quartz during the experiment.

Dislocation mobility around fluid inclusions during deformation is controlled by the interaction of dislocations with strain-free water bubbles. In the region outside of the fracture plane, with a relatively low density of water bubbles, the dislocations are free to move (glide) under the action of differential stress. On the other hand, in the healed fracture regions, high bubble concentrations impede dislocation motion, decreasing their mobility. In this region, dislocation glide is limited and dislocation climb is observed. Dislocation climb is enhanced by rapid precipitation of water bubbles on dislocation cores and by low strain rates during inclusion recovery.

Fluid inclusions that were overpressured exhibit a highly variable deformation behavior that is related to mechanical properties of the original inclusion. Before reequilibration and after the 30 day reequilibration experiment, some fluid inclusions show a high density of preexisting fracture dislocations. When overpressured, these inclusions are the most likely to leak by dislocation-induced water diffusion, and diffusion will be the primary mechanism of inclusion reequilibration. This mechanism is referred to as *diffusion-enhanced reequilibration*. On the other hand, some inclusions show a low number of fracture dislocations connected to the inclusion walls, but a relatively high number of wall dislocations. When overpressured, these inclusions deformed by water-assisted stretching of the inclusion walls, and this mechanism is referred to as *stretching-enhanced reequilibration*. Obviously, although either stretching or diffusion may dominate in a given fluid inclusion, both mechanisms are likely to contribute to the overall deformation process. Finally, some inclusions show no visible lattice defects in the surrounding quartz. Before deformation can begin, these inclusions must first develop dislocations in the host. Consequently, deformation of these inclusions may require some incubation period during which dislocations are developed on the inclusion walls.

After reequilibration for 180 days, a majority of the fluid inclusions showed the same fluid density or homogenization temperature (Fig. 2; see also Vityk and Bodnar 1998) and similar microstructures. This indicates that after 180 days of overpressure, original mechanical heterogeneities were eliminated. The implication of this observation is that regardless of the mechanism of inclusion deformation (either diffusion or stretching reequilibration) or the original mechanical properties (e.g. large inclusions vs small inclusions), all inclusions eventually recover from high internal stresses to become similar in terms of homogenization temperature and microstructures.

Our results indicate that even relatively fast experimental loading rates allow synthetic fluid inclusions in natural Brazilian quartz to recover (chemically and volumetrically) such that internal stresses probably never reach the point where the inclusions fail by brittle fracture. A similar conclusion was reached by Küster and Stöckert (1997) based on results of a fluid inclusion study of high P, low T rocks from Crete. The driving force for fluid inclusion recovery involves two related mechanisms: plastic deformation of hydrolytically weakened wet quartz in the healed fracture, and water leakage associated with preexisting and strain-induced dislocations. Studies of natural samples conducted by Bakker and Jansen (1993) and Kronenberg et al. (1986) indicate that similar processes may be involved in inclusion reequilibration in nature, suggesting that laboratory data from synthetic inclusions can be used to interpret results from natural fluid inclusions.

Acknowledgements The authors wish to thank P. Cordier, C. Invernizzi and J. Student for helpful discussions during the course of this work. Reviews of an earlier version of this manuscript by Ron Bakker and an anonymous reviewer are greatly appreciated. Funding for this work was provided by National Science Foundation Grant # EAR9526668.

References

Audédat A, Günther D (1999) Mobility and H_2O loss from fluid inclusions in natural quartz crystals. Contrib Mineral Petrol 137: 1–14

Bakker RJ, Jansen JBH (1990) Preferential water leakage from fluid inclusions by means of mobile dislocations. Nature 345: 58–60

Bakker RJ, Jansen JBH (1991) Experimental post-entrapment water loss from synthetic CO_2-H_2O inclusions in natural quartz. Geochim Cosmochim Acta 55: 2215–2230

Bakker RJ, Jansen JBH (1993) Calculated fluid evolution path versus fluid inclusion data in the COHN system as exemplified by metamorphic rocks from Rogaland, south-west Norway. J Metamorphic Geol 11: 357–370

Bakker RJ, Jansen JBH (1994) A mechanism for preferential H_2O leakage from fluid inclusions in quartz, based on TEM observations. Contrib Mineral Petrol 116: 7–20

Barker AJ (1995) Post-entrapment modification of fluid inclusions due to overpressure: evidence from natural samples. J Metamorphic Geol 13: 737–750

Bodnar RJ (1993) Revised equation and table for determining the freezing point depression of H_2O-NaCl solutions. Geochim Cosmochim Acta 57: 683–684

Bodnar RJ, Bethke PM (1984) Systematics of stretching of fluid inclusions. I. Fluorite and sphalerite at 1 atmosphere confining pressure. Econ Geol 79: 141–161

Bodnar RJ, Sterner SM (1987) Synthetic fluid inclusions. In: Barnes HL, Ulmer GC (eds) Hydrothermal experimental techniques. Wiley and Sons, New York, pp 423–457

Bodnar RJ, Vityk MO (1994) Interpretation of microthermometric data for NaCl-H_2O fluid inclusions. In: De Vivo B, Frezzotti ML (eds) Fluid inclusions in minerals: methods and applications. Virginia Polytechnic Inst and State Univ, Blacksburg, VA, pp 117–131

Bodnar RJ, Binns PR, Hall DL (1989) Synthetic fluid inclusions. VI. Quantitative evaluation of the decrepitation behavior of fluid inclusions in quartz at one atmosphere confining pressure. J Metamorphic Geol 7: 229–242

Boullier AM, Michot G, Pêcher A, Barres O (1989) Diffusion and plastic deformation around fluid inclusions in synthetic quartz. In: Bridgwater D (ed) Fluid movements – element transport and the composition of the deep crust. (NATO ASI Series, 281) Kluwer, Dordrecht, pp 345–360

Cordier P, Doukhan JC (1989) Water solubility in quartz and its influence on ductility. Eur J Mineral 1: 221–237

Cordier P, Doukhan JC, Ramboz C (1994) Influence of dislocations on water leakage from fluid inclusions in quartz: a quantitative reappraisal. Eur J Mineral 6: 745–752

Doukhan JC, Trepied L (1985) Plastic deformation of single quartz crystals. Bull Mineral 108: 97–123

Gerretsen J, Paterson MS, McLaren AC (1989) The uptake and solubility of water in quartz at elevated pressure and temperature. Phys Chem Miner 16: 334–342

Gerretsen J, McLaren AC, Paterson MS (1993) Evolution of inclusions in wet synthetic quartz as a function of temperature and pressure; implication for water weakening. In: Boland JN, FitzGerald JD (eds) Defects and processes in the solid state: geosciences application, McLaren vol. Elsevier Science Publisher, Amsterdam, pp 27–47

Gratier JP, Jenatton L (1984) Deformation by solution-deposition and re-equilibration of fluid inclusions in crystals depending on temperature, internal pressure, and stress. J Struct Geol 6: 189–200

Griggs DT, Blacic JD (1964) The strength of quartz in the ductile regime. EOS Trans Am Geophys Union 45: 102–103

Griggs DT, Blacic JD (1965) Anomalous weakness of synthetic crystals. Science 147: 292–295

Guilhaumou N, County R, Dahan N (1987) Deformation of fluid inclusions in fluorite under confining pressure. Chem Geol 61: 47–53

Hall DL, Bodnar RJ (1990) Methane in fluid inclusions from granulites: a product of hydrogen diffusion? Geochim Cosmochim Acta 54: 641–652

Hall DL, Sterner SM (1993) Preferential water loss from synthetic fluid inclusions. Contrib Mineral Petrol 114: 489–500

Hall DL, Sterner SM (1995) Experimental diffusion of hydrogen into synthetic fluid inclusions in quartz. J Metamorphic Geol 13: 345–355

Hollister LS (1990) Enrichment of CO_2 in fluid inclusions in quartz by removal of H_2O during crystal-plastic deformation. J Struct Geol 12: 895–901

Johnson EL, Hollister LS (1995) Syndeformational fluid trapping in quartz: determining the pressure-temperature conditions of deformation from fluid inclusions and the formation of pure CO_2 fluid inclusions during grain-boundary migration. J Metamorphic Geol 13: 239–249

Kerrich R (1976) Some effects of tectonic recrystallization on fluid inclusions in vein quartz. Contrib Mineral Petrol 59: 195–202

Kotel'nikova ZA (1994) The response of fluid inclusions to changes in physicochemical parameters in the external medium (in Russian). Geokhimia 4: 476–485

Kronenberg AK (1994) Hydrogen speciations and chemical weakening of quartz. In: Heaney PJ, Prewitt CT, Gibbs GV (eds) Silica. (Reviews in mineralogy, vol 29) Mineral Soc Am, Washington, DC, pp 123–176

Kronenberg AK, Kirby SH, Aines RD, Rossman GR (1986) Solubility and diffusional uptake of hydrogen in quartz at high water pressures: implication to hydrolytic weakening. J Geoph Res 91: 12723–12744

Küster M, Stöckert B (1997) Density changes of fluid inclusions in high-pressure low-temperature metamorphic rocks from Crete: a thermobarometric approach based on the creep strength of the host minerals. Lithos 41: 151–167

Larson LT, Miller JD, Nadeau JE, Roedder E (1973) Two sources of error in low temperature inclusion homogenization determination and corrections on published temperatures for the East Tennessee and Laisvall deposits. Econ Geol 68: 113–116

Lawler JP, Crawford ML (1983) Stretching of fluid inclusions resulting from a low temperature microthermometric technique. Econ Geol 78: 527–529

Leroy J (1979) Contribution à l'étalonnage de la pression interne des inclusions fluides lors de leur décrépitation. Bull Soc Fr Minéral Cristallogr 102: 584–593

Mavrogenes JA, Bodnar RJ (1994) Hydrogen movement into and out of fluid inclusions in quartz: experimental evidence and geologic implications. Geochim Cosmochim Acta 58: 141–148

McLaren AC, Cook RF, Hyde ST, Tobin RC (1983) The mechanism of the formation and growth of water bubbles and associated dislocation loops in synthetic quartz. Phys Chem Miner 9: 79–94

McLaren AC, FitzGerald JD, Gerretsen J (1989) Dislocation nucleation and multiplication in synthetic quartz: relevance to water weakening. Phys Chem Miner 15: 465–482

Pêcher A (1981) Experimental decrepitation and re-equilibration of fluid inclusions in synthetic quartz. Tectonophysics 78: 567–583

Pêcher A, Boullier AM (1984) Evolution à pression et température élevées d'inclusions fluides dans un quartz synthétique. Bull Mineral 107: 139–153

Poland EL (1982) Stretching of fluid inclusions at confining pressures up to 1 kilobar. MS thesis, Berkeley, Univ California

Prezbindowski DR, Larese RE (1987) Experimental stretching of fluid inclusions in calcite – implications for diagenetic studies. Geology 15: 333–336

Sterner SM, Bodnar RJ (1986) Re-equilibration of fluid inclusions in quartz at elevated temperatures and pressures: the role of H_2O diffusion (abstract). EOS Am Geophys Union 67: 407

Sterner SM, Bodnar RJ (1989) Synthetic fluid inclusions. VII. Re-equilibration of fluid inclusions in quartz during laboratory simulated metamorphic burial and uplift. J Metamorphic Geol 7: 243–260

Sterner SM, Hall DL, Bodnar RJ (1988) Post-entrapment compositional changes in fluid inclusions: experimental evidence for water diffusion in quartz (abstract). Geol Soc Am Abstr Program 20: A100

Sterner SM, Hall DL, Keppler H (1995) Compositional re-equilibration of fluid inclusions in quartz. Contrib Mineral Petrol 119: 1–15

Swanenberg HEC (1980) Fluid inclusions in high-grade metamorphic rocks from S.W. Norway. Geol Ultraiectina 25

Ulrich MR, Bodnar RJ (1988) Systematics of stretching of fluid inclusions. II. Barite at one atmosphere confining pressure. Econ Geol 83: 1037–1046

Vityk MO, Bodnar RJ (1995a) Do fluid inclusions in high grade metamorphic terranes preserve peak metamorphic density during retrograde decompression? Am Mineral 80: 641–644

Vityk MO, Bodnar RJ (1995b) Textural evolution of synthetic fluid inclusions in quartz during re-equilibration, with applications to tectonic reconstruction. Contrib Mineral Petrol 121: 309–323

Vityk MO, Bodnar RJ (1998) Statistical microthermometry of synthetic fluid inclusions in quartz during decompression. Contrib Mineral Petrol 132: 149–162

Vityk MO, Bodnar RJ, Dudok IV (1995) Natural and synthetic re-equilibration textures of fluid inclusions in "Marmarosh Diamonds": evidence of refilling under conditions of compressive loading. Eur J Mineral 7: 1071–1087

Wanamaker BJ, Evans B (1989) Mechanical re-equilibration of fluid inclusions in San Carlos olivine by power-law creep. Contrib Mineral Petrol 102: 102–111

Wilkins RWT, Barkas JP (1978) Fluid inclusion deformation and recrystallization in granite tectonites. Contrib Mineral Petrol 65: 293–299

Wilkins RWT, Bird JR, Ewald AH (1981) Observations on deformation microstructures and fluid inclusions in proton-irradiated halite. Neues Jahrb Mineral Abh 141: 240–257